Complex behavior in a simple system: Low-temperature Ag/Ag(100) growth revisited

Yunsic Shim and Jacques G. Amar
Department of Physics & Astronomy, University of Toledo, Toledo, Ohio 43606, USA
(Received 13 August 2009; revised manuscript received 13 November 2009; published 14 January 2010)

The experimentally observed nonmonotonic temperature dependence of the surface roughness in Ag/Ag(100) growth over the temperature range $T=55-180$ K is examined. In general, we find that the surface roughness depends sensitively on a competition between a variety of low-barrier processes including downward funneling of depositing atoms, island relaxation via edge zipping and edge diffusion, atom attraction, and concerted interlayer diffusion at kinks. The short-range attraction of depositing atoms to microprotrusions also plays a crucial role in determining the surface roughness, especially at low temperature. By taking these processes into account in our simulations, good agreement with experiment is obtained over the entire temperature range.

DOI: 10.1103/PhysRevB.81.045416 PACS number(s): 68.55.−a, 81.15.Aa

I. INTRODUCTION

Recently, there has been a great deal of progress in understanding the morphological evolution in epitaxial thin-film growth (for a recent review see Ref. 1), and a variety of effects and processes have been shown to play an important role. In addition to growth temperature, deposition flux, and deposition angle,[2–11] these include the effects of crystal geometry,[12,13] the Ehrlich-Schwoebel (ES) barrier to interlayer diffusion,[14] edge and corner diffusion,[15,16] and the attraction of depositing atoms to the substrate.[2–6,8,9,11,17–23] Understanding these effects is important since they can have a strong influence on a variety of important film properties including the surface morphology.

One case of particular interest is that of Ag/Ag(100) growth for which an unusually complex dependence of the surface roughness on deposition temperature has been observed over the temperature range $T=55-300$ K.[24] In particular, as the temperature was reduced below 300 K, the roughness of 25 monolayer (ML) films was found to first increase—with a peak at approximately 220 K—and then decrease as the temperature was further reduced. As the temperature was decreased below 135 K, the roughness again increased—with a second low-temperature peak at approximately 90 K—and then decreased again as the temperature was further reduced to 55 K.

By using a simplified kinetic Monte Carlo (KMC) model[24,25] which takes into account the existence of relatively small but nonzero barriers for downward funneling (DF) (Ref. 26) of atoms deposited at nonfourfold hollow sites (e.g., "restricted" DF), and which also assumes instantaneous island relaxation (e.g., perfectly "square" or spiral islands) the nonmonotonic behavior of the surface roughness at high temperature ($T=135-300$ K) has been explained by Stoldt *et al.*[24] In particular, the increase in the surface roughness as the temperature is decreased from 300 to 220 K was attributed to the increased effect of the ES barrier to interlayer diffusion as the temperature is decreased over this temperature range. Similarly, the decrease in the surface roughness as the temperature is further decreased from 220 to 135 K was explained by the increased role of DF (Ref. 26) of atoms deposited near step edges, due to the increased island and step density as the monomer diffusion rate decreases. However, the resulting model led to poor agreement with experiment below 135 K and was also unable to explain the experimentally observed decrease in the roughness below 90 K. In addition, it leads to predictions[24,25] for the low-temperature thin-film vacancy density which are more than an order of magnitude higher than the results of recent parallel temperature-accelerated dynamics (parTAD) simulations.[10]

One reason for the relatively poor agreement between the KMC results of Stoldt *et al.*[24] and experiment at low temperature is the assumption [24,27] of an instantaneous reconstruction of islands corresponding to rapid edge diffusion along close-packed island edges. While such an assumption leads to a computationally efficient algorithm, and is also expected to be valid at high temperatures ($T>150$ K), it also leads to square island-shapes even when edge diffusion is kinetically suppressed at low temperature. In addition, the inclusion of a relatively large activation barrier for DF from threefold hollow sites in this model leads to the suppression of DF at low temperature ($T<90$ K) along with an excessively high vacancy density. Furthermore, the model of Stoldt *et al.* does not take into account steering effects due to short-range (SR) attraction between depositing atoms and surfaces, which can affect the surface roughness even in the case of normal incidence[17,18] and which become increasingly important at low temperature.[6]

Here we show that by taking into account the existence of very low barriers for edge smoothing as well as for DF at threefold hollow sites, along with the effects of SR attraction of depositing atoms to microprotrusions, excellent quantitative agreement with experiment can be obtained over the temperature range $T=55-110$ K. Furthermore, by taking into account the existence of a variety of low barriers for concerted interlayer diffusion at and near kinks, which we have obtained by carrying out parallel temperature-accelerated dynamics[10] simulations for representative configurations found in our KMC simulations, both qualitative and quantitative agreement with experiment can be obtained over the entire low-temperature range ($T=55-180$ K). Due to the fact that our calculated barriers for DF from threefold hollow sites are significantly lower than previously obtained in Ref. 24, our model also leads to a negligible low-

temperature vacancy density in good agreement with recent accelerated dynamics simulations of low-temperature Cu/Cu(100) growth.[10] We note that since the model of Stoldt *et al.* already explains the experimental results reasonably well at high temperature ($T=135-300$ K), and also because our more detailed KMC simulations become increasingly computationally demanding with increasing temperature (due to the existence of repetitive low-barrier events such as edge diffusion and edge zipping), here we restrict ourselves to the temperature range $T=55-180$ K.

The organization of this paper is as follows. In Sec. II, we first describe the hybrid kinetic Monte Carlo model used in our simulations to take into account the effects of SR attraction during deposition. This includes a summary of the key activation barriers for intralayer diffusion as well as for DF and concerted interlayer diffusion at kinks. We note that since the barriers for intralayer diffusion were previously calculated in Ref. 32 using the Adams, Foiles, and Wolfer (AFW) (Ref. 28) embedded-atom-method (EAM) (Ref. 29) potential, in our model we have primarily used these values. However, we have also carried out additional parallel accelerated dynamics simulations of typical configurations using the Voter-Chen (VC) EAM potential,[30] and the resulting barriers for DF and concerted interlayer diffusion at kinks are also presented. In Sec. III, we then present a comparison between our simulation results and experimental results over the temperature range $T=55-180$ K. In addition, we discuss the effects of SR attraction as well as of a variety of low-barrier processes—including edge diffusion, edge zipping, atom attraction, and concerted interlayer diffusion at kinks—on the surface morphology. Finally, in Sec. IV, we discuss the effects of edge-diffusion barrier on the surface roughness and summarize our results.

II. KINETIC MONTE CARLO MODEL

A. Deposition

In order to include the SR attraction of depositing atoms to the surface, in our simulations we have used a hybrid model which combines a one-atom molecular-dynamics (MD) simulation of the deposition process with KMC simulations of activated events. As in previous work,[18] we assume that the depositing atom is launched normally from a random position above the substrate at a height equal to that of the highest point of the film plus the cutoff distance r_{cut}. Similarly, we assume that the initial kinetic energy of the deposited atom corresponds to the average value $\bar{K}_i=2k_BT_m \simeq 0.2$ eV, where k_B is Boltzmann's constant and $T_m \approx 1235$ K is the melting temperature of Ag. The depositing atom is then assumed to follow the trajectory determined by its interaction with the substrate with the substrate atoms held fixed in their lattice positions. Once its distance to the closest substrate atom is equal to the nearest-neighbor distance, it is then placed at the nearest empty fcc lattice site, and assumed to undergo DF until it reaches a "stable" site with a barrier for interlayer diffusion. We note that in recent simulations of normal-incidence Cu/Cu(100) growth at $T=160$ K,[6] the surface roughness obtained using this method was found to be only slightly lower than that obtained by carrying out a full MD simulation of the depositing atom and surrounding substrate. In order to check for the dependence on interaction potential, our MD simulations were carried out using two different potentials: the VC EAM potential[30] as well as a Lennard-Jones (LJ) Ag potential[31] with the same cutoff ($r_{cut}=3\sigma$ with $\sigma=2.644$ Å) as the EAM potential. In order to compare with the experiment of Ref. 24, our simulations were carried out using the experimental deposition rate of 0.02 ML/s.

B. Activated events

In our KMC model we have considered three different types of activated processes: intralayer diffusion, interlayer diffusion of atoms at nonfourfold hollow sites (e.g., restricted DF or RDF), and interlayer diffusion of atoms at fourfold hollow sites. We first discuss the case of intralayer diffusion.

1. Intralayer diffusion

With the exception of a few processes discussed below, all barriers for intralayer diffusion were obtained from the results of EAM calculations by Mehl *et al.*[32] in which the activation energies were calculated as a function of the occupation numbers of the 7 sites surrounding the moving atom labeled 1 through 7 [see Fig. 1(a)(0)]. However, since the effect of sites 6 and 7 on the activation barrier is relatively weak, for simplicity in our KMC model we have only used the occupation numbers of sites 1–5, and have assumed that sites 6 and 7 are empty.

Figures 1(a) and 1(b) show some of the key low-barrier intralayer activated processes which are active on the time scale of the experimental deposition rate for $T<150$ K. In particular, as shown in Figs. 1(a)(i) and 1(a)(ii), there exists a very low barrier of 0.16 eV for a monomer to be "attracted" to an empty site with two lateral bonds (edge zipping). Such "edge-zipping" processes tend to enhance the regularity of step edges thus suppressing DF. Also shown in Fig. 1(b) are somewhat higher-barrier processes corresponding to edge diffusion. However, for the case shown in Fig. 1(b) (i) of an edge-diffusing atom with one in-plane bond, a barrier of 0.30 eV has been previously calculated using density-functional theory (DFT).[33] Therefore, in this case we have used the DFT value, rather than the lower EAM value (0.22 eV) calculated in Ref. 32. Since the activation energy for the related process of "atom attraction" shown in Fig. 1(b)(ii) is expected to be similar, a comparable value of 0.3 eV has also been assumed for this process. However, as discussed in Sec. IV, for comparison we have also carried out simulations with energy barriers for singly bonded edge diffusion and atom attraction obtained from AFW (Ref. 28) and Voter-Chen[30] EAM potentials. We note that these barriers are all significantly lower than the barrier[33] (0.45 eV) for monomer diffusion on a flat terrace, which does not become active until approximately 180 K.

In order to properly take into account island relaxation at higher temperatures, as shown in Fig. 1(c) we also include an effective barrier for corner rounding (which becomes active

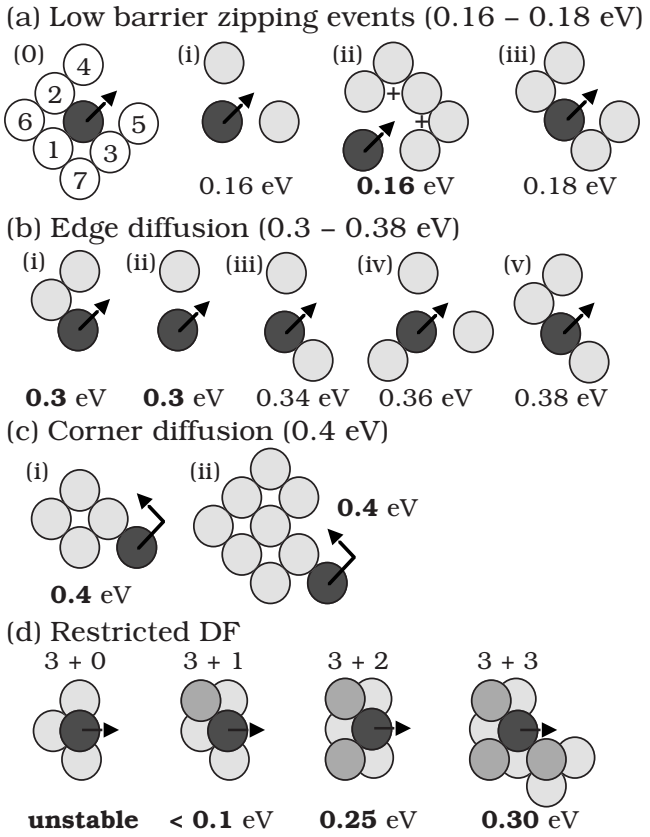

FIG. 1. Key low-barrier activated processes (boldface) for intralayer diffusion and DF: (a) low-barrier edge zipping, (b) higher-barrier processes including (i) edge diffusion and (ii) atom attraction. (c) corner diffusion, (d) DF for atoms at threefold hollow sites. Also shown in (b)(iii)–(b)(v) are some representative higher-barrier processes. Sites labeled "+" in (a)(ii) indicate threefold hollow sites which are converted to fourfold hollow sites by edge zipping.

on the time scale of deposition at approximately 150 K) using the value (0.40 eV) estimated by Thiel and Evans in Ref. 41. For simplicity, we do not distinguish between (i) global corner rounding and (ii) kink rounding in our simulations. In addition to the processes shown in Fig. 1, our model includes a variety of other intralayer diffusion processes with higher activation barriers.[32] However, since the barriers for these moves are all greater than 0.45 eV, they are only relevant above 165 K. As assumed by Mehl *et al.*,[32] we have used a prefactor of 10^{12} s^{-1} for all intralayer diffusion events.

2. Barriers for restricted DF

Since the DF of atoms deposited at nonfourfold hollow sites may be suppressed at low temperatures,[24] we have carried out parallel temperature-accelerated dynamics simulations using the Voter-Chen[30] EAM potential in order to determine the relevant energy barriers. Figure 1(d) shows the key low-barrier activated processes for DF included in our KMC simulations which become active over the temperature range 55–110 K. As in Ref. 24, we assume that DF is effectively instantaneous for atoms deposited at nonfourfold hollow sites with coordination number $m<3$ (where m is the number of nearest neighbors for a given atom) as well as for atoms with $m=3$ on (111) microfacets, since the barriers for these transitions are less than 0.1 eV. Based on similar observations, we also assume instantaneous DF for atoms with only two support sites, regardless of the number of in-plane bonds. However, in contrast to Ref. 24, in which DF barriers of 0.15 eV (0.25 eV) were assumed for atoms at sites with three supporting atoms and 0(1) lateral bond, respectively, here we assume that DF is essentially instantaneous for such sites, since our EAM calculations yield values less than 0.1 eV. In addition, our EAM calculations for atoms at threefold support sites with two in-plane lateral bonds (3+2) yield a range of energy barriers (0.22–0.27 eV) with an average value of approximately 0.25 eV, depending on the presence of additional atoms in their neighborhood. Thus, in agreement with Ref. 24, we also assume that for the 3+2 configurations, the barrier for DF is 0.25 eV, while we have found that the barrier for atoms with threefold support sites with three in-plane lateral bonds is somewhat larger (0.30 eV). We note that this 3+3 configuration has not been considered in Ref. 24. In addition to those configurations, we have also considered 3+4 configurations [not shown in Fig. 1(a)] with a barrier of 0.35 eV, but their effects on the surface morphology are very minimal. As for the case of intralayer diffusion, we have assumed a prefactor of 10^{12} s^{-1} for all RDF events.

3. Interlayer diffusion

As in the KMC simulations of Stoldt *et al.*,[24] in our KMC simulations we have included a barrier of 0.51 eV for monomer descent at close-packed step edges. However, assuming a prefactor of 10^{12} s^{-1}, this process does not become active on the time scale of the experimental deposition rate except for $T>180$ K, and so is not relevant over the temperature range of our simulations. However, while our KMC simulations without interlayer diffusion are in good agreement with the experimental results of Ref. 24 at low T, for $T>110$ K the simulated roughness is significantly higher than the experimental value (see Fig. 3). This suggests that some additional low-barrier interlayer diffusion process or processes which were not included in Ref. 24 may play an important role in reducing the surface roughness for $T>110$ K.

In order to determine the relevant activation barriers for such processes, we have carried out parTAD simulations for representative configurations obtained from our KMC simulations using the Voter-Chen[30] EAM potential for Ag. As can be seen in Fig. 2, our simulations indicate the existence of a variety of low-barrier interlayer diffusion processes for the concerted interlayer diffusion of atoms at single and double kink sites—with energy barriers ranging from 0.2 eV [for a monomer at a double kink with a "forward" atom in the layer below, see Fig. 2(a)(i)] to 0.58 eV [for an atom which is part of a trimer without a forward atom in the layer below, see Fig. 2(c)(ii)]. In addition, we note that the dominant interlayer diffusion processes observed in our KMC simulations (in boldface in Fig. 2) correspond to activation barriers ranging from 0.28 eV [Fig. 2(a)(iii)] to 0.37 eV [Fig. 2(b)(iv)]. In particular, while the 0.3 eV interlayer diffusion process for a monomer at an open step edge shown in Fig. 2(a)(iv)—for which the activation barrier has been previously calculated by Kurpick and Rahman in Ref. 34—plays an important role,

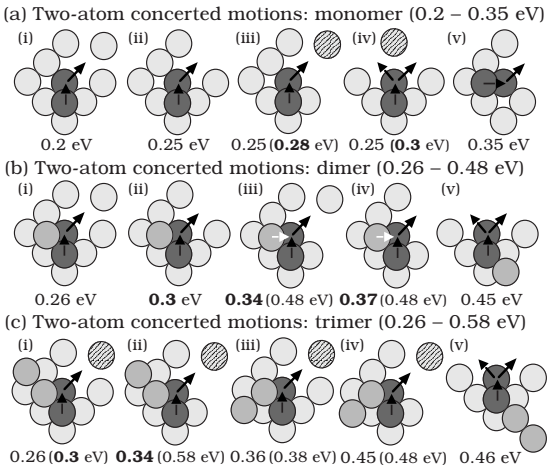

FIG. 2. Low-barrier interlayer diffusion processes for (a) monomers (b) dimers, and (c) trimers near kinks which become active above 110 K. Activation barriers in boldface correspond to dominant processes observed in KMC simulations. Barriers in parentheses in (b) correspond to motion of "upper atom" (white arrow) "away from kink." Barriers in parentheses in (c) correspond to configurations without cross-hatched atom.

the even lower-barrier process shown in Fig. 2(a)(iii) is also important. In addition, due to the high dimer and trimer density over this temperature range, the low-barrier "dimer" and "trimer" interlayer diffusion processes shown in Figs. 2(b)(ii)–2(b)(iv) an2(c)(ii) also play important roles. We note that for some of the configurations shown in Fig. 2, a range of activation energies was obtained in our parTAD simulations, due to differences in the representative configurations at longer ranges. In this case, an average value was used for the activation barrier.

Interestingly, the origin of the low activation barriers shown in Fig. 2 is the same as for edge diffusion and edge zipping, e.g., the existence of "side atoms" which can attract the displaced atoms as they move to their new sites. Accordingly, as shown in Fig. 2, the interlayer diffusion barrier is even lower when there are two attracting side atoms corresponding to a "double kink" rather than one. This clearly illustrates the effects of long-range interactions in determining the energy barrier of a concerted interlayer diffusion event. We have also calculated the corresponding Vineyard prefactors[35] for most of the interlayer diffusion events and the resulting prefactors range from a lowest value of 4.0×10^{12} s^{-1} to a maximum value of 2.3×10^{13} s^{-1} with an average prefactor of 1.0×10^{13} s^{-1}. Accordingly, a prefactor of 10^{13} s^{-1} was assumed for all interlayer diffusion moves.[36,37]

Thus, in addition to the SR attraction of depositing atoms to the substrate, our model includes the following processes: (i) DF for atoms with $m \leq 3$ as well as for atoms at 3+1 sites and all twofold hollow sites. (ii) Restricted DF with an activation barrier of 0.25 eV (0.30 eV) for atoms at threefold hollow sites with 2 (3) in-plane bonds. (iii) Low-barrier edge zipping and edge diffusion. (iv) Low-barrier concerted processes for interlayer diffusion at kinks.

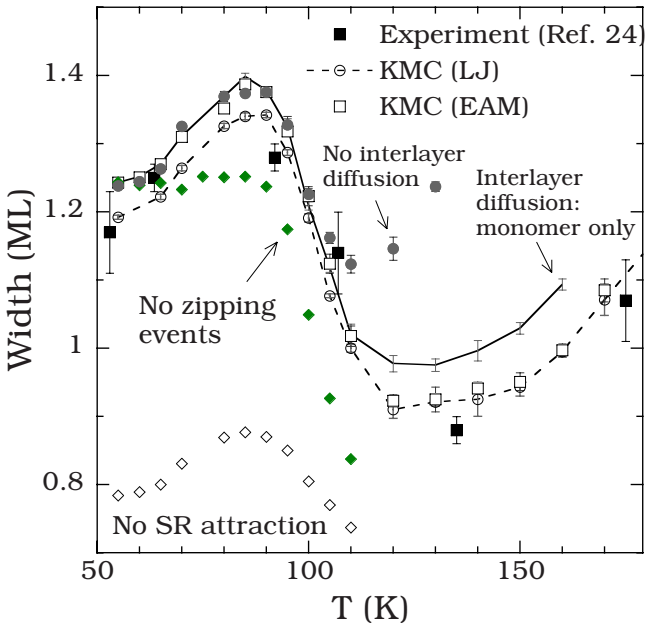

FIG. 3. (Color online) Comparison between simulations and experimental results (filled squares) for surface roughness at 25 ML as function of deposition temperature. Open squares (circles) correspond to hybrid KMC simulations using EAM (LJ) potential for simulating the deposition process. Filled circles correspond to simulations without the concerted low-barrier interlayer diffusion processes shown in Fig. 2. Solid line corresponds to inclusion of only monomer interlayer diffusion [Fig. 2(a)].

III. RESULTS

Figure 3 shows a comparison between our KMC simulation results for the surface roughness at 25 ML (open squares) with the corresponding experimental results of Stoldt *et al.*[24] (filled squares). As can be seen, while the simulated roughness is slightly higher than the experimental roughness at low T, in general there is good qualitative and quantitative agreement with experiment over the entire temperature range $T=55-180$ K. In particular, there is a peak in the surface roughness at low temperature ($T \simeq 85$ K) as well as a minimum in the surface roughness at higher temperature ($T \simeq 135$ K) in good qualitative agreement with experiment.

We first consider the low-temperature behavior since this has not been previously explained. Within the context of our KMC model this peak can be explained as follows. As the temperature is decreased from 110 to 85 K the DF of atoms deposited at "3+3" sites (with activation energy of 0.3 eV) is first suppressed at 110 K, followed by the suppression of DF at "3+2" sites at 90 K, thus leading to an increase in the surface roughness. However, as the temperature is further reduced below 85 K, the very-low-barrier edge-zipping mechanism—which can convert threefold hollow sites to stable fourfold hollow sites, as shown in Fig. 1(a)(ii)—is also suppressed. This leads to an increase in the amount of DF at "3+0" and "3+1" sites, thus leading to a decrease in the surface roughness. In contrast, if we remove the low-barrier zipping events from our model (see Fig. 3), then the surface roughness increases approximately monotonically with decreasing temperature over this temperature range. This be-

havior is very similar to that found in Ref. 24 using a model which does not take into account the effects of SR attraction or the existence of finite barriers for edge smoothing. This indicates that the inclusion of low-barrier zipping events is crucial to explain the experimentally observed nonmonotonic behavior at low T. Also shown in Fig. 3 are results obtained at low T in the absence of SR attraction. While the experimentally observed nonmonotonic behavior is still reproduced in this case, the surface roughness is significantly lower than in experiment, thus indicating that the attraction of depositing atoms to microprotrusions also plays a crucial role in determining the surface roughness.

We now consider the temperature range from 110 to 135 K. We note that over this temperature range both edge diffusion and atom attraction become active, even though terrace diffusion of isolated monomers and interlayer diffusion at close-packed step edges remain inactive. In particular, due to the increased effects of edge diffusion, which tends to regularize step edges and thus reduce DF, in the absence of low-barrier mechanisms for interlayer diffusion one expects the surface roughness to increase with increasing temperature over this temperature range (see the case of no interlayer diffusion in Fig. 3). This is in contrast to the experimental results of Ref. 24 which indicate a further decrease in the roughness. However, by including in our simulations the low-barrier concerted interlayer diffusion processes for monomers, dimers, and trimers near kinks shown in Fig. 2, good agreement with experiment is obtained as shown in Fig. 3. In contrast, if we take into account only the "monomer" processes for interlayer diffusion at kinks shown in Fig. 2(a) and exclude dimer and trimer interlayer diffusion at kinks, then there is a systematic deviation from the experimental results for $T>120$ K. Thus, our results indicate that the low-barrier mechanisms for concerted interlayer diffusion at kinks shown in Fig. 2 play a crucial role in explaining the decrease in the surface roughness with increasing temperature over the temperature range $T=110-135$ K.

In order to further compare with the experiments of Ref. 24, we also consider the dependence of the surface roughness on temperature for $T>135$ K. As can be seen in Fig. 3, the surface roughness obtained in our KMC simulations, increases with increasing temperature over this temperature range in good agreement with experiment. We note that this increase in roughness is due in part to the increased effects of edge diffusion and edge zipping as well as to the activation of corner diffusion (which occurs at approximately 150 K) since all of these effects suppress interlayer diffusion by decreasing the kink density. Atom attraction [see Fig. 1(b)(ii)] also plays a role since this tends to suppress interlayer diffusion at kinks by attracting monomers at step edges away from the step edge to form dimers and trimers.

Besides the dependence of the surface roughness w on temperature at 25 ML, it is also interesting to consider the dependence on film thickness, along with the associated growth exponent β (where $w\sim\langle h\rangle^{\beta}$ with $\langle h\rangle$ being the average film height) and its dependence on growth temperature. As can be seen in Fig. 4, as the temperature increases from 60 to 90 K, both the roughness and the value of β increase slightly. However, a further increase in temperature to 130 K results in a significant drop in the overall surface width as

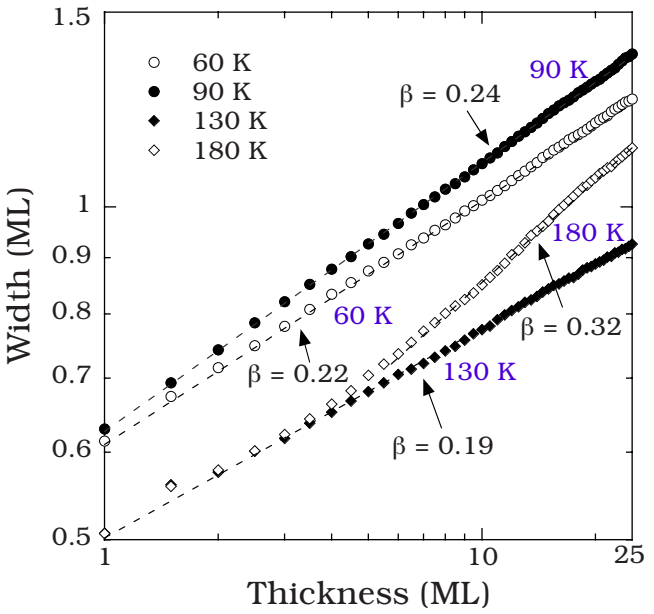

FIG. 4. (Color online) Surface width vs film thickness using EAM potential for deposition at four representative temperatures, $T=60$, 90, 130, and 180 K.

well as a slightly lower value of β ($\beta=0.19$) due to the activation of DF events and interlayer diffusion. Finally, an increase in the growth temperature to 180 K leads to an increase in the effective growth exponent to a value ($\beta=0.32$) which is significantly larger than 1/4. We note that this is close to but still somewhat lower than the experimental value ($\beta\simeq0.4$) found at $T=190$ K.[38]

Figure 5 shows the corresponding pictures of the surface morphology at a thickness of 25 ML. As can be seen, the lateral feature size increases with increasing temperature. In particular, while all intralayer events are suppressed at 60 K [see Fig. 5(a)] with the activation of DF from 3+2 sites as well as very fast edge zipping above 85 K, relatively long one-dimensional islands aligned along the ⟨110⟩ directions begin to appear [see Fig. 5(b)]. As the temperature increases further, both single-bond edge diffusion and low-barrier concerted interlayer diffusion processes at kinks become active. This leads to the formation of somewhat square islands with very few small islands on top of them, as shown in Fig. 5(c). Finally, at $T=180$ K, corner rounding is active while monomer diffusion is just becoming active. As a result, the mounds formed during growth are larger and more regular. We note that the relatively well-developed mound structures shown in Fig. 5(d) for $T=180$ K are similar to those observed in the scanning tunneling microscopy (STM) picture of surface morphology at slightly higher temperature ($T=190$ K).[39]

Thus, our results indicate that over the temperature range from 55 to 180 K, both the surface roughness and the surface morphology depend sensitively on a competition between a variety of low-barrier processes including DF, interlayer diffusion at kinks, edge diffusion, edge zipping, and atom attraction. In particular, the existence of low-barrier interlayer diffusion processes for monomers, dimers, and trimers near kinks turns out to be crucial to explain the observed tempera-

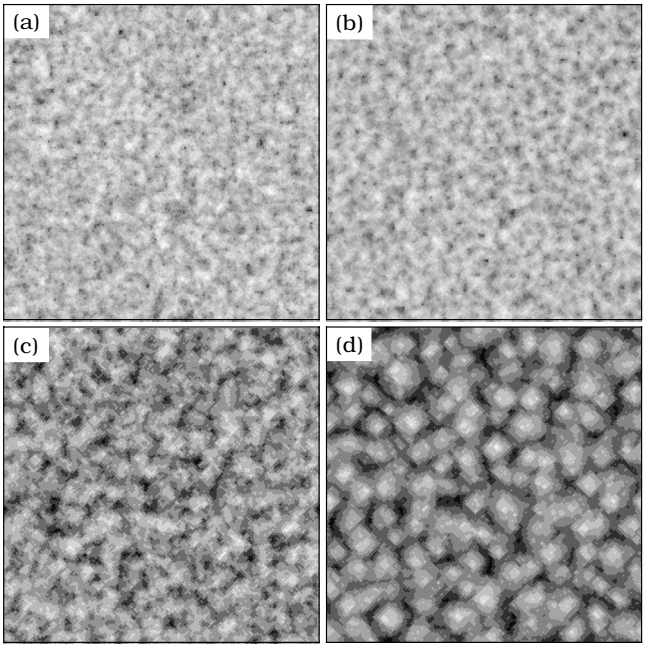

FIG. 5. Gray-scale pictures of surface morphology at four temperatures (a) 60 K, (b) 90 K, (c) 130 K, and (d) 180 K with $L=256$ at 25 ML, obtained using deposition with the VC EAM potential.

ture dependence of the surface roughness at higher temperatures. In general, we expect that similar mechanisms are likely to play a significant role in understanding a variety of other metal(100) systems.

IV. DISCUSSION

Using a hybrid KMC model which takes into account the effects of SR attraction of depositing atoms to the substrate, as well as the existence of low-barrier processes for DF, island relaxation, edge smoothing, and concerted interlayer diffusion at kinks, we have carried out simulations of Ag/Ag(100) growth over the temperature range $T=50-180$ K. Using this model we have obtained good qualitative and quantitative agreement with the experimental results of Stoldt *et al.*[24] for the nonmonotonic dependence of the surface roughness on temperature. This includes the existence of a low-temperature roughness peak at approximately $T=85$ K, which had not previously been explained, as well as the existence of a minimum in the surface roughness at approximately 130 K.

In particular, our results indicate that the low-temperature peak can be explained as follows. As the temperature is decreased from 130 to 85 K, the roughness at first increases due to the suppression of low-barrier mechanisms for interlayer diffusion at kinks, and then increases further due to the suppression of DF at 3+2 sites, as previously discussed in Ref. 24. In contrast, the subsequent decrease in the roughness as the temperature is decreased below 85 K, is due to the existence of very-low-barrier processes for DF at 3+0 and 3+1 sites (which remain active even at low temperatures) combined with the suppression of edge zipping, which tends to eliminate such DF sites. Our simulation results also indicate that SR attraction plays a crucial role in enhancing the surface roughness, especially at low temperature.

Our results also indicate that over the temperature range from 110 to 180 K, the surface roughness depends sensitively on a competition between a variety of low-barrier processes including interlayer diffusion at kinks, edge diffusion, edge zipping, and atom attraction. We note that this picture differs significantly from that given in Ref. 24 in which instantaneous island relaxation was assumed, along with a single effective global barrier for monomer interlayer diffusion. In particular, our results indicate that the existence of low-barrier interlayer diffusion processes for monomers, dimers, and trimers at kinks is crucial to explain the observed behavior at higher temperatures. We have also found that the inclusion of a relatively small barrier for corner diffusion (which tends to increase the surface roughness by decreasing the kink density) is crucial in order to obtain good agreement with experiment for $T>150$ K.

As already noted, in our simulations we have primarily used energy barriers obtained from EAM potentials since these are generally expected to be quite accurate for metals. In particular, the barriers for edge zipping and other interlayer diffusion processes previously calculated by Mehl *et al.*[32] using an AFW EAM potential were used while we have used a Voter-Chen EAM potential to calculate the barriers for interlayer diffusion at kinks. However, since more accurate DFT values were available[33] for monomer diffusion and edge diffusion, in these two cases we have used the DFT values rather than the EAM values of Ref. 32, while the barrier for atom attraction was assumed to be equal to the DFT value for edge diffusion for consistency. Therefore, it may be of interest to consider how our results would be altered if instead the EAM values for edge diffusion and atom attraction were used.[40]

Figure 6 shows a comparison between the experimental results and those obtained using a model in which the EAM barrier values calculated in Ref. 32 for edge diffusion ($E_e=0.22$ eV) and atom attraction ($E_a=0.23$ eV) were used. As can be seen, in this case the roughness is significantly higher than the experimental value for $T>95$ K. Poor agreement with experiment is also obtained (see Fig. 6) if instead we assume a somewhat higher value ($E_e=0.25$ eV) as has been suggested in Ref. 41. These results suggest that the correct value of the edge-diffusion barrier is significantly larger than the value ($E_e=0.22$ eV) calculated in Ref. 32 and indeed closer to the DFT value ($E_e=0.30$ eV) used in our simulations.

One possible explanation for this is related to the fact that with increasing temperature islands become bigger while their edges become straighter and longer, as is evident from the STM pictures shown in Refs. 24 and 39. Accordingly, the edge-diffusion barrier calculated in Ref. 32 may not be appropriate at higher temperatures since these calculations only considered interactions up to next-nearest neighbors [see Fig. 1(a)(0)]. In this connection, we note that calculations by Voter,[42] indicate that the edge-diffusion barrier increases with island-edge length and island size, presumably due to the combined effects of long-range interactions and island relaxation. This is also consistent with the fact that the DFT

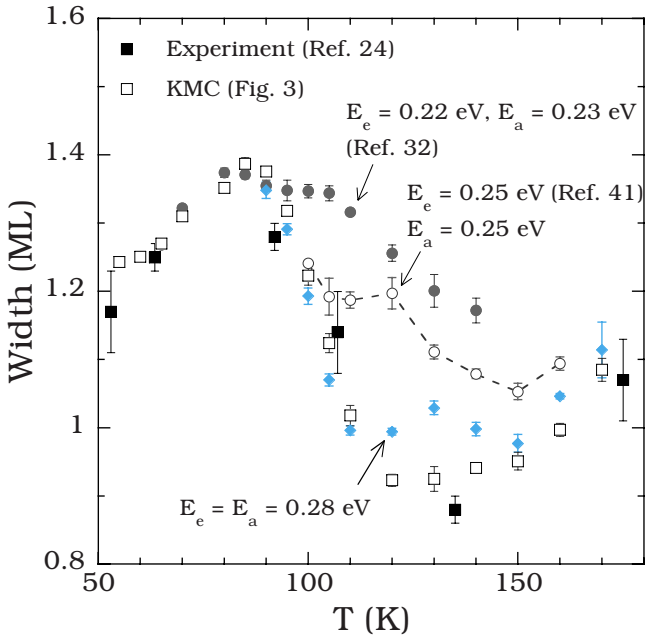

FIG. 6. (Color online) Surface width at 25 ML obtained using different values of energy barriers for edge diffusion (E_e) and atom attraction (E_a) (see text). Open squares (KMC Fig. 3) correspond to simulation results already shown in Fig. 3 using an EAM potential for simulating the deposition process.

barriers for edge diffusion calculated in Ref. 33 (E_e =0.27 eV for generalized gradient approximation and 0.3 eV for local-density approximation) correspond to edge diffusion along an infinitely long island edge. Thus, it is perhaps not surprising that the simulation results in Fig. 6 with higher values of the edge-diffusion barrier (E_e=0.28 eV and E_e=0.30 eV) are in significantly better agreement with experiment than those with significantly lower values of the edge-diffusion barrier.

In conclusion, we have shown that the dependence of the surface roughness in Ag/Ag(100) growth over the temperature range 55–180 K can be quantitatively explained by taking into account the existence of low-barrier processes for step-edge smoothing, DF, and interlayer diffusion, as well as the SR attraction of depositing atoms to microprotrusions. In particular, while the increase in the roughness as the temperature is decreased from 110 to 90 K is due to the suppression of DF of atoms deposited at 3+2 and 3+3 sites, the subsequent decrease in the roughness as the temperature is reduced below 90 K is due to the suppression of edge zipping along with the existence of low-barrier processes for DF. In contrast, the decrease in the surface roughness as the growth temperature is increased from 110 to 135 K is primarily due to the existence of low-barrier processes for interlayer diffusion at kinks which "turn on" over this temperature range. Finally, for $T>135$ K the increased effects of edge diffusion lead to a decreased kink density which suppresses the low-barrier mechanisms for interlayer diffusion resulting in an increase in the roughness with increasing temperature. It is the complex interplay between all of these different processes which leads to the nonmonotonic temperature dependence observed in experiment.

ACKNOWLEDGMENTS

We would like to acknowledge useful discussions with Art Voter. This work was supported by NSF under Grants No. DMR-0606307 and DMR-0907399, as well as by a grant of computer time from the Ohio Supercomputer Center.

[1] J. W. Evans, P. A. Thiel, and M. C. Bartelt, Surf. Sci. Rep. **61**, 1 (2006).
[2] S. van Dijken, L. C. Jorritsma, and B. Poelsema, Phys. Rev. Lett. **82**, 4038 (1999).
[3] S. van Dijken, L. C. Jorritsma, and B. Poelsema, Phys. Rev. B **61**, 14047 (2000).
[4] J. Seo, S.-M. Kwon, H.-Y. Kim, and J.-S. Kim, Phys. Rev. B **67**, 121402(R) (2003).
[5] J. Seo, H.-Y. Kim, and J.-S. Kim, Phys. Rev. B **71**, 075414 (2005).
[6] V. Borovikov, Y. Shim, and J. G. Amar, Phys. Rev. B **76**, 241401(R) (2007).
[7] Y. Shim and J. G. Amar, Phys. Rev. Lett. **98**, 046103 (2007).
[8] J. Seo, H.-Y. Kim, and J.-S. Kim, J. Phys.: Condens. Matter **19**, 486001 (2007).
[9] Y. Shim, V. Borovikov, and J. G. Amar, Phys. Rev. B **77**, 235423 (2008).
[10] Y. Shim, V. Borovikov, B. P. Uberuaga, A. F. Voter, and J. G. Amar, Phys. Rev. Lett. **101**, 116101 (2008).
[11] Y. Shim, M. E. Mills, V. Borovikov, and J. G. Amar, Phys. Rev. E **79**, 051604 (2009).
[12] M. C. Bartelt and J. W. Evans, Phys. Rev. Lett. **75**, 4250 (1995).
[13] J. G. Amar and F. Family, Phys. Rev. B **54**, 14742 (1996).
[14] G. Ehrlich and F. Hudda, J. Chem. Phys. **44**, 1039 (1966); R. L. Schwoebel, J. Appl. Phys. **40**, 614 (1969).
[15] M. V. Ramana Murty and B. H. Cooper, Phys. Rev. Lett. **83**, 352 (1999).
[16] O. Pierre-Louis, M. R. D'Orsogna, and T. L. Einstein, Phys. Rev. Lett. **82**, 3661 (1999).
[17] F. Montalenti and A. F. Voter, Phys. Rev. B **64**, 081401(R) (2001).
[18] J. Yu and J. G. Amar, Phys. Rev. Lett. **89**, 286103 (2002).
[19] J. G. Amar, Phys. Rev. B **67**, 165425 (2003).
[20] J. G. Yu, J. G. Amar, and A. Bogicevic, Phys. Rev. B **69**, 113406 (2004).
[21] J. Yu and J. G. Amar, Phys. Rev. B **69**, 045426 (2004).
[22] F. Rabbering, H. Wormeester, F. Everts, and B. Poelsema, Phys. Rev. B **79**, 075402 (2009).
[23] F. Rabbering, A. Kara, H. Wormeester, T. Warnaar, O. Trushin, T. S. Rahman, and B. Poelsema, Phys. Rev. Lett. **103**, 096105 (2009).
[24] C. R. Stoldt, K. J. Caspersen, M. C. Bartelt, C. J. Jenks, J. W. Evans, and P. A. Thiel, Phys. Rev. Lett. **85**, 800 (2000).
[25] K. J. Caspersen and J. W. Evans, Phys. Rev. B **64**, 075401

(2001).
[26] J. W. Evans, D. E. Sanders, P. A. Thiel, and A. E. DePristo, Phys. Rev. B **41**, R5410 (1990).
[27] M. C. Bartelt and J. W. Evans, Surf. Sci. **423**, 189 (1999).
[28] J. B. Adams, S. M. Foiles, and W. G. Wolfer, J. Mater. Res. **4**, 102 (1989).
[29] S. M. Foiles, M. I. Baskes, and M. S. Daw, Phys. Rev. B **33**, 7983 (1986).
[30] A. F. Voter and S. P. Chen, MRS Symposia Proceedings No. 82 (Materials Research Society, Pittsburgh, 1987), p. 175; A. F. Voter, in *Intermetallic Compounds: Principles and Practice*, edited by J. H. Westbrook and R. L. Fleischer (Wiley & Sons, New York, 1995), Vol. 1, p. 77.
[31] P. Cuan, D. R. Mckenzie, and B. A. Pailthope, J. Phys.: Condens. Matter **8**, 8753 (1996).
[32] H. Mehl, O. Biham, I. Furman, and M. Karimi, Phys. Rev. B **60**, 2106 (1999).
[33] B. D. Yu and M. Scheffler, Phys. Rev. Lett. **77**, 1095 (1996).
[34] U. Kurpick and T. S. Rahman, Phys. Rev. B **57**, 2482 (1998).
[35] G. H. Vineyard, J. Phys. Chem. Solids **3**, 121 (1957).
[36] In agreement with previous results for the dynamical prefactors in Cu/Cu(100) intralayer diffusion obtained by Yildirim *et al.* (Ref. 37) we find that there is very little correlation between the prefactor and energy barrier.
[37] H. Yildirim, A. Kara, S. Durukanoglu, and T. S. Rahman, Surf. Sci. **600**, 484 (2006).
[38] K. J. Caspersen, A. R. Layson, C. R. Stoldt, V. Fournee, P. A. Thiel, and J. W. Evans, Phys. Rev. B **65**, 193407 (2002).
[39] K. J. Caspersen, C. R. Stoldt, A. R. Layson, M. C. Bartelt, P. A. Thiel, and J. W. Evans, Phys. Rev. B **63**, 085401 (2001).
[40] We note that over this temperature range, monomer diffusion does not play a significant role and so the difference between the DFT and EAM values does not have a significant effect.
[41] P. A. Thiel and J. W. Evans, J. Phys. Chem. B **108**, 1428 (2004).
[42] A. F. Voter, Proc. SPIE **821**, 214 (1987).